

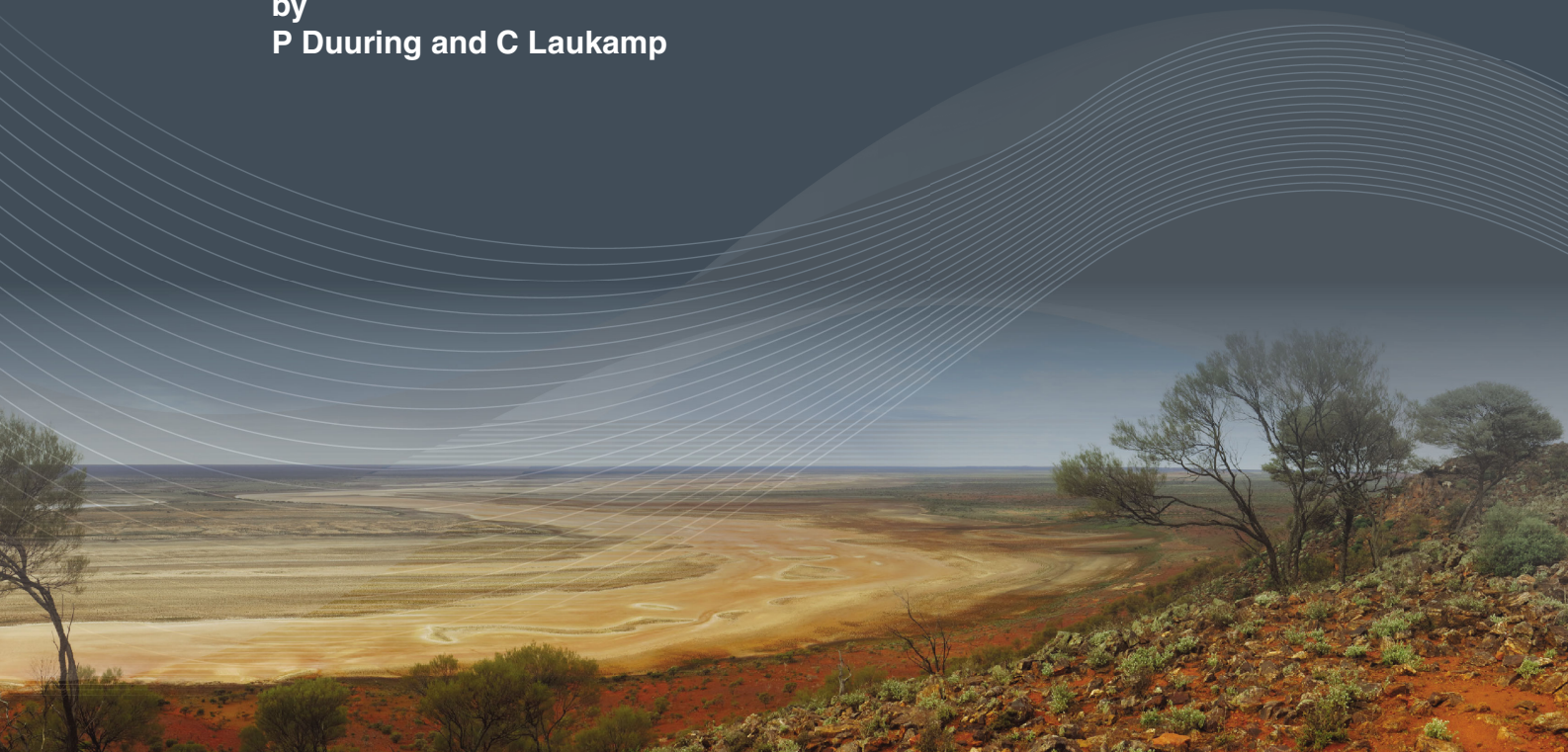


Government of Western Australia  
Department of Mines and Petroleum

RECORD 2016/18

# MAPPING IRON ORE ALTERATION PATTERNS IN BANDED IRON-FORMATION USING HYPERSPECTRAL DATA: DRILLHOLE PK11DD001, MT RICHARDSON, YILGARN CRATON, WESTERN AUSTRALIA

by  
P Duuring and C Laukamp



Geological Survey of  
Western Australia



EXPLORATION  
INCENTIVE SCHEME





Government of **Western Australia**  
Department of **Mines and Petroleum**

**Record 2016/18**

# **MAPPING IRON ORE ALTERATION PATTERNS IN BANDED IRON-FORMATION USING HYPERSPECTRAL DATA: DRILLHOLE PK11DD001, MT RICHARDSON, YILGARN CRATON, WESTERN AUSTRALIA**

by

**P Duuring and C Laukamp<sup>1</sup>**

<sup>1</sup> Western Australian Centre of Excellence for 3D Mineral Mapping, CSIRO Mineral Resources, 26 Dick Perry Avenue, Kensington WA 6151

**Perth 2016**



**Geological Survey of  
Western Australia**

**MINISTER FOR MINES AND PETROLEUM**  
**Hon. Sean K L'Estrange MLA**

**ACTING DIRECTOR GENERAL, DEPARTMENT OF MINES AND PETROLEUM**  
**Tim Griffin**

**EXECUTIVE DIRECTOR, GEOLOGICAL SURVEY OF WESTERN AUSTRALIA**  
**Rick Rogerson**

#### **REFERENCE**

**The recommended reference for this publication is:**

Duuring P and Laukamp C 2016, Mapping iron ore alteration patterns in banded iron-formation using hyperspectral data: drillhole PK11DD001, Mt Richardson, Yilgarn Craton, Western Australia: Geological Survey of Western Australia, Record 2016/18, 15p.

**National Library of Australia Card Number and ISBN 978-1-74168-721-7**

Grid references in this publication refer to the Geocentric Datum of Australia 1994 (GDA94). Locations mentioned in the text are referenced using Map Grid Australia (MGA) coordinates, Zone 50. All locations are quoted to at least the nearest 100 m.



#### **Disclaimer**

This product was produced using information from various sources. The Department of Mines and Petroleum (DMP) and the State cannot guarantee the accuracy, currency or completeness of the information. DMP and the State accept no responsibility and disclaim all liability for any loss, damage or costs incurred as a result of any use of or reliance whether wholly or in part upon the information provided in this publication or incorporated into it by reference.

#### **Published 2016 by Geological Survey of Western Australia**

This Record is published in digital format (PDF) and is available online at <[www.dmp.wa.gov.au/GSWApublications](http://www.dmp.wa.gov.au/GSWApublications)>.

#### **Further details of geological products and maps produced by the Geological Survey of Western Australia are available from:**

Information Centre  
Department of Mines and Petroleum  
100 Plain Street  
EAST PERTH WESTERN AUSTRALIA 6004  
Telephone: +61 8 9222 3459 Facsimile: +61 8 9222 3444  
[www.dmp.wa.gov.au/GSWApublications](http://www.dmp.wa.gov.au/GSWApublications)

**Cover image:** Elongate salt lake on the Yilgarn Craton — part of the Moore–Monger paleovalley — here viewed from the top of Wownaminia Hill, 20 km southeast of Yalgoo, Murchison Goldfields. Photograph taken by I Zibra for the Geological Survey of Western Australia

## Contents

Abstract .....	1
Introduction.....	1
Geological overview of the Mt Richardson prospect.....	1
Results from conventional logging of diamond drillhole PK11DD001.....	5
Rock types.....	5
Hypogene alteration of BIF.....	5
Hypogene alteration of mafic igneous rocks.....	6
Supergene alteration of BIF.....	6
Supergene alteration of mafic igneous rocks .....	6
Results of hyperspectral data acquisition and processing .....	6
Method .....	6
Rock types .....	10
Hypogene alteration of BIF.....	10
Hypogene alteration of mafic igneous rocks.....	10
Supergene alteration of BIF .....	10
Supergene alteration of mafic igneous rocks .....	10
Conclusions.....	13
Acknowledgements .....	13
References .....	13

## Appendix

Description of spectral scripts for geoscience products .....	15
---------------------------------------------------------------	----

## Figures

1. Iron ore occurrences in the Yilgarn Craton and location of diamond drillhole PK11DD001 .....	2
2. Solid geology map of the Mt Richardson prospect .....	4
3. Summary log for drillhole PK11DD001 showing hyperspectral data .....	7
4. Whole-rock and hyperspectral data for mafic igneous rocks .....	9
5. Hyperspectral data for BIF macrobands: key indices for alteration styles .....	11
6. Hyperspectral data for dolerite: chlorite abundance and chemistry .....	12
7. Hyperspectral data showing a comparison of kaolinite crystallinity .....	12



# Mapping iron ore alteration patterns in banded iron-formation using hyperspectral data: drillhole PK11DD001, Mt Richardson, Yilgarn Craton, Western Australia

by

P Duuring and C Laukamp<sup>1</sup>

## Abstract

The PK11DD001 diamond drillhole is located in the Parker area of the Mt Richardson iron prospect, Southern Cross Domain of the Yilgarn Craton. Drillhole PK11DD001 demonstrates the effects of late supergene alteration on the mineralogy and mineral chemistry of protoliths and their hypogene alteration mineral assemblages. The drillhole intersects one main banded iron-formation (BIF) macroband and several other thinner bands separated by dolerite. Two main compositional groups are identified in dolerite based on a comparison of their  $\text{Al}_2\text{O}_3/\text{TiO}_2$  ratios. The whole-rock MgO content of fresh, least-altered dolerite mirrors the Fe/Mg ratios of primary amphiboles and metamorphic chlorite detected by the SWIR spectrometer. Fresh examples of least-altered BIF are distinguished from fresh dolerite by the presence of amphibole, pyroxene, or plagioclase in dolerite. However, intense supergene alteration prevents the accurate identification of these protoliths. Hypogene alteration in BIF is defined by the addition of magnetite and quartz to primary BIF. These alteration zones correspond with moderate increases in  $\text{Fe}_{\text{total}}$ , but they display similar  $\text{SiO}_2$  contents to least-altered BIF due to the addition of hypogene quartz. Hypogene alteration zones in dolerite are characterized by coincident increases in the 'chlorite abundance' and decreases in 'amphibole abundance' spectral signatures within about 15 m of BIF-hosted iron ore zones. Furthermore, chlorite compositions in dolerite become more Mg rich with proximity to these ore zones. Later supergene alteration resulted in a decrease in quartz abundance due to its replacement by goethite, corresponding to an increase in the 'ferric oxides abundance' and decrease in the 'quartz abundance' spectral signatures of BIF. Supergene alteration of BIF has been vital for producing the economic upgrade of iron grades in hypogene ore zones at Mt Richardson.

**KEYWORDS:** banded iron-formation, hypogene deposits, iron ores, spectral analysis, supergene alteration

## Introduction

Reflectance spectral data were collected by the HyLogger-3 for six diamond drillholes from four iron ore deposits located in various greenstone belts throughout the Yilgarn Craton. The sites of interest include the Weld Range (drillhole WRRD0583; Duuring and Laukamp, 2016a), Windarling (drillhole W2DDH007; Duuring and Laukamp, 2016b), Koolyanobbing, and Mt Richardson iron camps (Fig. 1). The aim is to identify hypogene and supergene alteration minerals associated with high-grade iron ore (>57 wt%  $\text{Fe}_{\text{total}}$ ) in banded iron-formation (BIF) and nearby mafic country rocks. For this purpose, three diamond drillholes were selected for study from the

Mt Richardson prospect (PK11DD001, PK12DD001, and PI12DD002). The drillholes intersect multiple BIF macrobands and diverse styles of hypogene and supergene alteration in BIF and mafic igneous country rocks. Hyperspectral data from the PK11DD001 drillhole have previously been reported and interpreted by Chiarelli (2015). This present study re-examines the reported hyperspectral dataset of Chiarelli (2015) and provides additional comparison plots of hyperspectral data and new interpretations.

## Geological overview of the Mt Richardson prospect

The geology of the Mt Richardson prospect has been documented in an unpublished study by Duuring and Hagemann (2013); a summary of that work is given here.

---

<sup>1</sup> Western Australian Centre of Excellence for 3D Mineral Mapping, CSIRO Mineral Resources, 26 Dick Perry Avenue, Kensington WA 6151

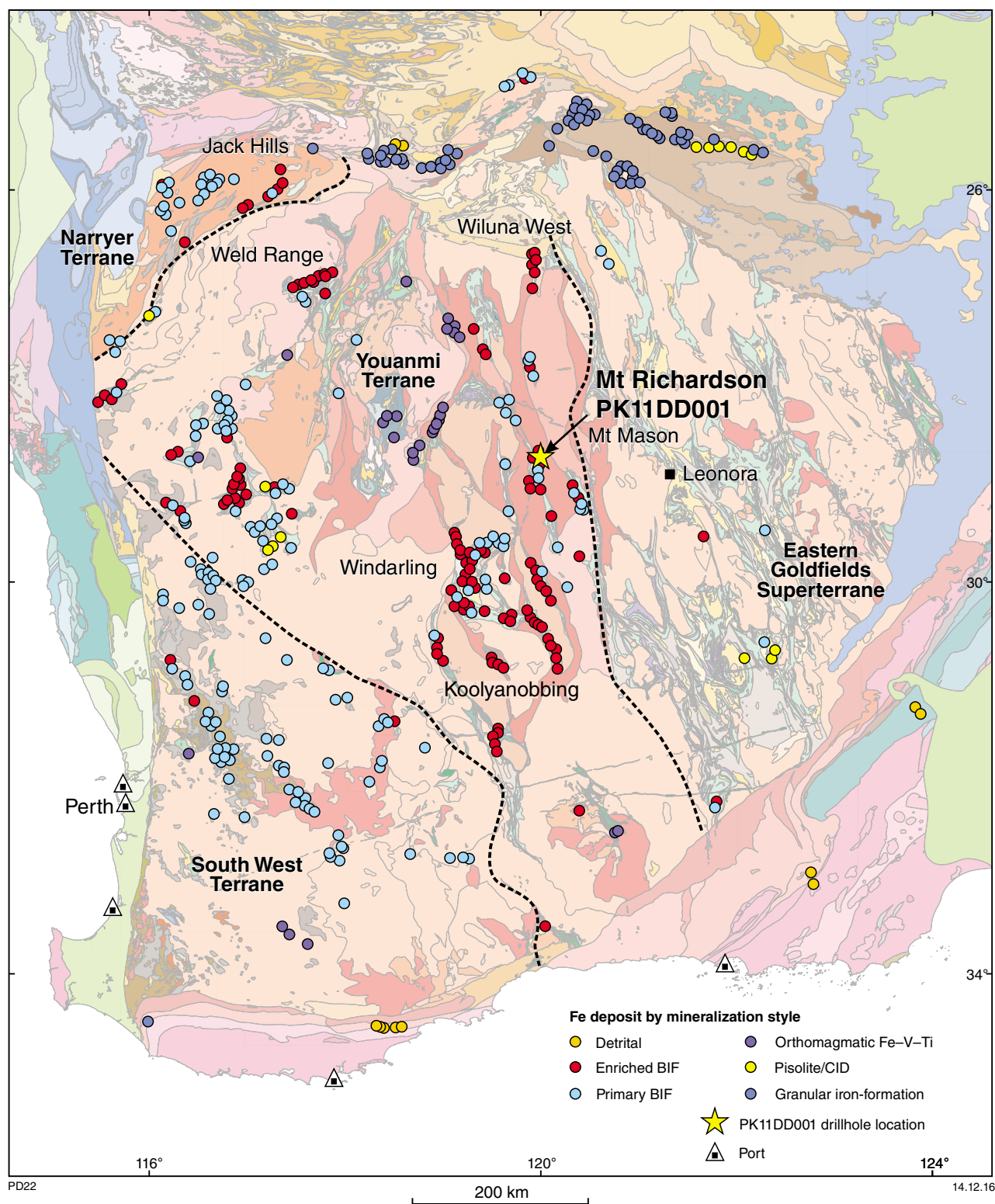


Figure 1. Distribution of iron ore occurrences in the Yilgarn Craton and location of diamond drillhole PK11DD001 in the Mt Richardson district. Regional geological map from GSWA (2016); iron ore deposits from the GSWA MINEDEX database <[www.dmp.wa.gov.au/minedex](http://www.dmp.wa.gov.au/minedex)>. CID – channel iron deposit

The Mt Richardson BIF-hosted iron ore prospect is located in the Southern Cross Domain of the Yilgarn Craton, approximately 530 km northeast of Perth and 130 km west of Leonora (Fig. 1). The prospect contains at least 11 BIF macrobands that are 5–90 m thick, steeply west-dipping, and extend along a north-northwest strike (Fig. 2). Mafic igneous rocks separate the individual BIF bands. Goethite–hematite-rich, high-grade ore zones are locally hosted by all exposed BIF bands in the prospect, although the western bands host iron ore zones that are laterally more continuous (Fig. 2).

All rocks in the Mt Richardson prospect are metamorphosed to upper greenschist facies; the prefix ‘meta’ applies to all rocks mentioned hereafter but has been omitted from rock descriptions for brevity. Primary stratigraphic relationships in the Mt Richardson prospect area are complicated by complex folding and faulting. Macroscopic fold hinges defined by BIF are preferentially exposed along ridges within the range, with narrower fold limbs commonly faulted and truncated.

BIF macrobands comprise alternating mesobands (1–30 mm thick) of primary iron oxides and quartz. Iron oxide bands commonly represent up to 40 vol% of least-altered BIF, although BIF may grade into banded chert along strike away from the Mt Richardson prospect. Fresh examples of mafic igneous rocks intersected by drillholes include komatiitic basalt, high-Mg tholeiitic basalt, and high-Fe tholeiitic basalt. Texturally, these rocks vary from basalt to dolerite and gabbro. Least-altered, high-Fe tholeiitic basalt comprises primary igneous plagioclase, primary and metamorphic amphiboles, and metamorphic and hydrothermal chlorite and epidote. The margins of most BIF macrobands are intensely weathered and deformed, preventing definitive interpretation of these igneous units as extrusive flows, intrusive units, or a combination of both. A 1–10 m thick blanket of transported sediment covers weathered mafic rocks and BIF along the flanks of most ridges in the Mt Richardson prospect. The detrital unit is poorly sorted and contains subrounded to angular fragments of BIF and mafic igneous rocks cemented by fine-grained goethite.

Bedding in the Mt Richardson prospect strikes north to north-northwest and mainly dips 60–90° west to west-southwest. Four generations of folds are preserved in BIF. The earliest generation of folds is only rarely persevered in outcrop as centimetre-scale, isoclinal F<sub>1</sub> folds that are refolded by the more commonly expressed upright and tight F<sub>2</sub> folds. The limbs of F<sub>2</sub> folds are deformed by 0.1 – 1 m wide, south-striking, steeply west-dipping, ductile shear zones and mylonite zones in BIF. The shear zones and mylonite zones are oriented subparallel to BIF macrobands and contacts with mafic igneous rocks. The timing of the shear zones in the mafic igneous rocks is uncertain, but it is likely there were several discrete episodes of deformation, demonstrated by the local granulation of early quartz veins within the shear zones.

All examples of BIF collected from drillcore and from the surface are at least slightly weathered, as demonstrated

by the common pseudomorphic replacement of primary magnetite by hematite (martitization) and the local replacement of these iron oxide minerals by supergene goethite. Least-weathered examples of BIF are best exposed in the easternmost BIF macrobands. In western areas, least-altered BIF is preserved in the centre of thick BIF macrobands, away from the more deformed margins of the BIF. Least-altered BIF mainly comprises 35–40 wt% Fe<sub>total</sub>, 38–50 wt% SiO<sub>2</sub>, 0.02 – 2.00 wt% Al<sub>2</sub>O<sub>3</sub>, 0.020 – 0.079 wt% P<sub>2</sub>O<sub>5</sub>, 0.005 – 0.030 wt% MgO, and 5–10 wt% loss on ignition (LOI) content.

Hypogene magnetite–talc alteration is present as veins and wallrock alteration associated with <2 m thick, ductile shear zones in BIF. These shear zones are primarily located along both margins of BIF macrobands. The disseminated magnetite and talc define wallrock alteration zones in BIF that extend up to 25 m away from these sheared margins. Hypogene magnetite–talc alteration zones are not enriched in Fe<sub>total</sub> relative to least-altered BIF, but these zones have lower competency and enhanced permeability. Fresh and intensely magnetite–talc-altered BIF comprises 32–46 wt% Fe<sub>total</sub>, 36–38 wt% SiO<sub>2</sub>, 0.14 – 6.00 wt% Al<sub>2</sub>O<sub>3</sub>, 0.010 – 0.230 wt% P<sub>2</sub>O<sub>5</sub>, and 0.01 – 0.18 wt% MgO. Later hypogene specularite alteration of BIF is widest and most intensely developed within the most westerly BIF macrobands in the Mt Richardson prospect. At the prospect scale, hypogene specularite alteration intensity in the BIF macrobands increases with strain and shearing intensities from east to west. BIF bands and earlier hypogene alteration zones are locally cut by several generations of 1–50 cm thick quartz ± carbonate ± pyrite veins.

Supergene alteration zones are located near surface and extend to greater depths along the deformed margins of BIF macrobands. In these areas, primary iron oxide bands and hypogene magnetite in BIF are oxidized to martite, whereas primary quartz bands are leached, or replaced by supergene goethite. The resulting supergene-altered BIF is iron rich and silica poor, with high porosity. Primary banding and secondary schistosity in BIF are destroyed by supergene alteration, resulting in a massive to fragmental-textured rock. Supergene-altered BIF comprises 58–69 wt% Fe<sub>total</sub>, 0.5 – 6.0 wt% SiO<sub>2</sub>, 0.16 – 5.00 wt% Al<sub>2</sub>O<sub>3</sub>, 0.010 – 0.090 wt% P<sub>2</sub>O<sub>5</sub>, and 0.02 – 0.06 wt% MgO.

Least-altered mafic rocks are massive and homogeneous. The rocks comprise mostly primary amphibole and plagioclase, with metamorphic chlorite and epidote. Hypogene alteration zones in mafic igneous rocks are proximal to mineralized BIF macrobands and are characterized by an increase in hypogene chlorite and a decrease in primary amphibole and plagioclase. Supergene alteration is intensely developed along the contacts of BIF, overprinting and obscuring hypogene alteration zonation patterns. In more distal areas, quartz–magnetite–pyrite shear veins cut basalt, and are in turn cut by quartz–carbonate veins.

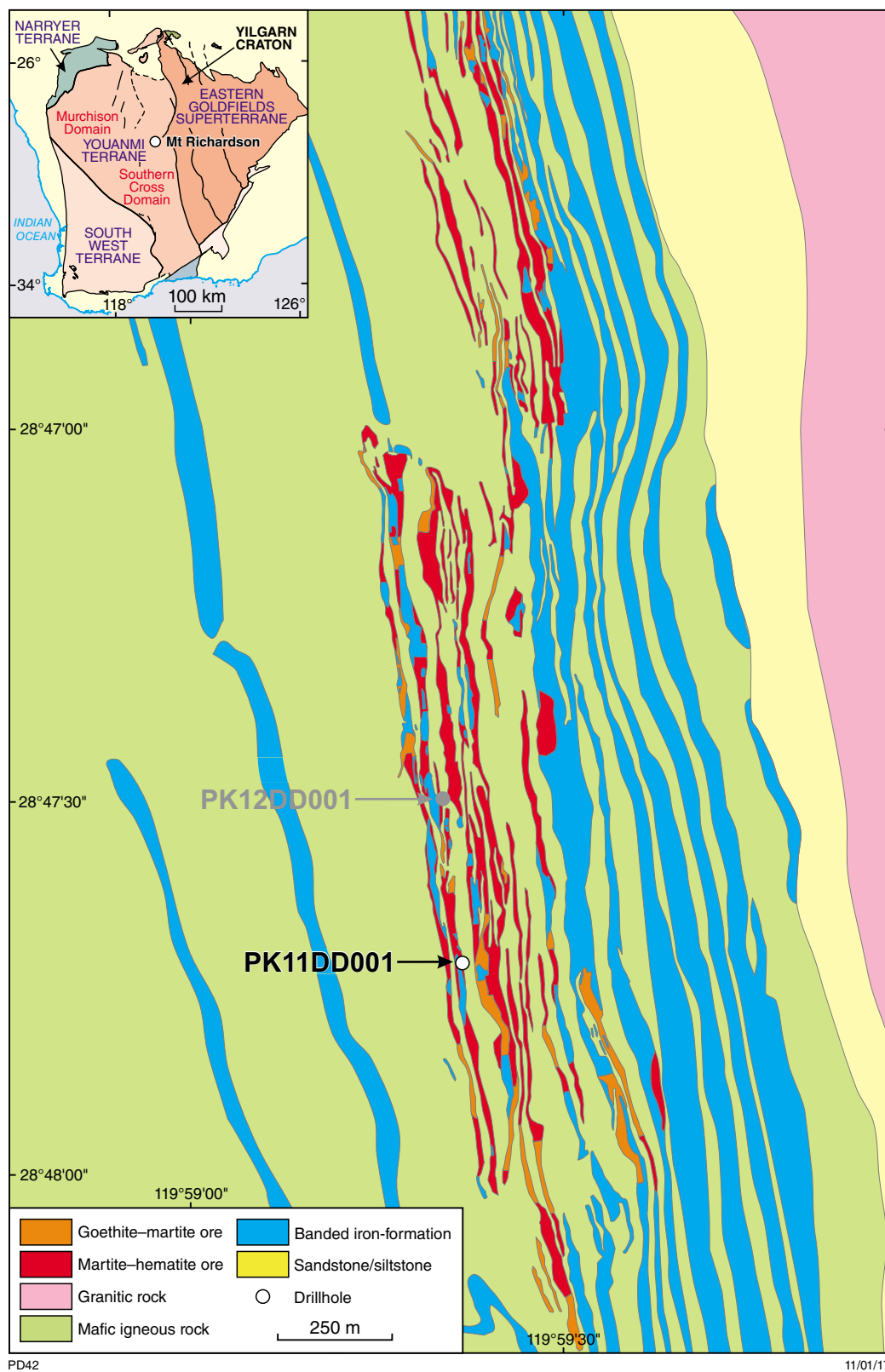


**Figure 2.** Solid geology map of the Mt Richardson prospect, showing the distribution of rock types, ore zones, and the location of drillhole PK11DD001

## Results from conventional logging of diamond drillhole PK11DD001

The PK11DD001 diamond drillhole, located in the Parker area of the Mt Richardson prospect (MGA 791815E 6811030 N), was drilled from the surface at an angle of  $-60^\circ$  towards  $090^\circ$  for a total length of 193.8 m. This drillhole was chosen based on its intersection of a thick BIF macroband and surrounding mafic igneous rocks. The BIF macroband records examples of fresh (i.e. unweathered), least-altered BIF, fresh, high-grade hypogene iron ore zones, and supergene-altered BIF. Neighbouring mafic igneous country rocks display a gradational trend from fresh, least-altered dolerite located near the base of the hole, towards intervals of hypogene alteration proximal to BIF, and to intensely supergene-altered rocks near the top of the drillhole.

The diamond drillcore was transported from its storage location at the Windarling mine site to the Perth Core Library in May 2013, where the core was cleaned, dried, and scanned using the HyLogger-3 by the Geological Survey of Western Australia (GSWA). The diamond drillcore was logged by conventional means, which included the documentation of relationships between rock types, textures, structures, and hypogene and supergene alteration mineral assemblages, and bulk-rock geochemistry. Drillhole PK11DD001 was returned to the Windarling mine site in April 2014.

### Rock types

The PK11DD001 drillhole intersects one main 53 m thick BIF macroband (hereafter referred to as BIF1) and five 1–3 m thick, BIF bands that are surrounded by dolerite and gabbro (Fig. 3). Least-altered BIF is located within the centre of the BIF1 macroband from about 47–74 m. The margins of this macroband are deformed and display intense hypogene and supergene alteration. Least-altered BIF comprises alternating 1–1.5 cm thick, quartz- and iron oxide-rich bands. Minor (5–10 vol%) disseminated grains of hypogene magnetite  $\pm$  specularite locally replace these primary bands. Minor, supergene, vitreous goethite, cryptocrystalline hematite, and martite partly (<10 vol%) replace diagenetic and hypogene magnetite in primary iron oxide-rich bands. Quartz-rich bands display minor replacement (5–10 vol%) by goethite. Least-altered BIF sampled from about 63 m depth is rich in  $\text{SiO}_2$  (44.94 wt%) and  $\text{Fe}_{\text{total}}$  (36.85 wt%), with minor  $\text{P}_2\text{O}_5$  (0.048 wt%), loss on ignition (LOI) content (2.02 wt%), and  $\text{Al}_2\text{O}_3$  (0.08 wt%). Intervals displaying elevated Ni, Co, Mn, Cu, and Zn at 55–60 m and 69–73 m most likely correspond to multiple, centimetre-thick occurrences of mafic igneous rocks within the BIF1 macroband (Fig. 3).

Least-altered dolerite from the Mafic4 interval (124–154 m) is dark green, massive, and medium grained (5–10 mm). The rock comprises primary amphibole and plagioclase, with metamorphic chlorite

and epidote. Least-altered Mafic4 consists mostly of  $\text{SiO}_2$  (52.02 – 55.50 wt%),  $\text{Al}_2\text{O}_3$  (11.43 – 12.35 wt%) and  $\text{Fe}_{\text{total}}$  (11.79 – 12.90 wt%), with minor  $\text{P}_2\text{O}_5$  (0.082 – 0.102 wt%), LOI content (1.03 – 1.73 wt%),  $\text{TiO}_2$  (1.32 – 1.61 wt%),  $\text{MgO}$  (3.12 – 4.33 wt%),  $\text{MnO}$  (0.12 – 0.18 wt%),  $\text{CaO}$  (5.25 – 8.14 wt%), and  $\text{K}_2\text{O}$  (0.15 – 0.23 wt%). The bulk-rock geochemistry of the Mafic4 dolerite indicates that it has a similar composition to a high-Fe tholeiitic basalt (Chiarelli, 2015).

A comparison of  $\text{Al}_2\text{O}_3$  vs  $\text{TiO}_2$  ratios for all intersected mafic igneous rocks shows similarities between the Mafic2 and Mafic4 intervals, as well as with a subset of the Mafic3b interval sampled from 94 to 112 m (Fig. 4a). These rocks are compositionally different from the Mafic1, Mafic5, Mafic6 intervals, and the Mafic3a interval sampled from 83 to 94 m (Fig. 4a). The two main groupings of immobile element ratios suggest that there are at least two genetically distinct mafic igneous protoliths intersected by the drillhole. The linear  $\text{Al}_2\text{O}_3$  vs  $\text{TiO}_2$  trends demonstrated by each mafic interval suggest fractionation of the magmas during crystallization (Fig. 4a). The irregular spatial distribution of these two compositional groups in the drillhole is best explained by the crystallization of the magmas as series of extrusive flows or intrusive sills, or the shear displacement or fold repetition of the mafic rocks (based on the common observation of shear zones and folded BIF bands throughout the drillcore).

### Hypogene alteration of BIF

The intensity of hypogene alteration in the BIF1 macroband increases from the centre to the margins (Fig. 3). The upper margin demonstrates the widest interval of hypogene alteration (from 27 to 47 m), compared with only a 3 m wide alteration zone along the lower margin (75–78 m). These hypogene-altered zones are intensely replaced by supergene alteration minerals within 1–5 m of the margins. Fresh examples of hypogene-altered BIF are dark grey to black, thinly banded, and display a moderately to strongly developed schistose fabric. These zones are rich in hypogene magnetite that is locally replaced by martite and is overgrown by later-forming specularite and microplaty hematite. Compared with least-altered BIF, the hypogene-altered BIF displays higher  $\text{Fe}_{\text{total}}$  (37.74 – 51.99 wt%),  $\text{P}_2\text{O}_5$  (0.042 – 0.185 wt%), and LOI content (2.12 – 5.48 wt%), but lower  $\text{SiO}_2$  (18.94 – 43.65 wt%), and comparable  $\text{Al}_2\text{O}_3$  (0.07 – 2.35 wt%) contents. The variable enrichments in  $\text{Fe}_{\text{total}}$  and  $\text{SiO}_2$  are the product of hypogene magnetite–quartz alteration of BIF. Matching local enrichments in  $\text{P}_2\text{O}_5$  and LOI contents are likely due to the weak goethite overprint of the hypogene alteration zones (e.g. at 43–44 m).

The narrower, 1–3 m thick, BIF2, BIF3, BIF4, BIF5, and BIF6 macrobands (Fig. 3) are moderately supergene altered. The BIF5 and BIF6 macrobands are schistose and moderately altered to hypogene magnetite  $\pm$  quartz, whereas the other narrow macrobands are unaffected by hypogene alteration.

## Hypogene alteration of mafic igneous rocks

Hypogene chlorite-altered dolerite coincides with the Mafic2, Mafic3, and part of the Mafic4 intervals, from 78 to 116 m (Fig. 3). Proximal hypogene alteration zones in the Mafic2 and Mafic3 intervals are partly obscured by a 7 m thick, intensely supergene-altered zone (from 78 to 85 m). There is moderate supergene alteration from 85 to 91 m, whereas fresh, proximal, alteration zones extend from 91 to 116 m. Proximal, hypogene, chlorite-rich alteration zones are green, fine grained, and schistose. Hypogene chlorite replaces primary amphibole, pyroxene, and plagioclase. Later quartz–carbonate veins and associated quartz–carbonate–epidote alteration locally (i.e. 91–116 m) replace chlorite-rich proximal alteration zones in dolerite.

Relative to more distal examples of fresh mafic igneous rocks (124–154 m), the proximal hypogene chlorite-rich alteration zones are enriched in LOI content (4.30 – 5.18 wt%) and MgO (5.52 – 6.80 wt%), depleted in CaO (0.28 – 0.53 wt%), and have comparable values for Fe<sub>total</sub> (11.73 – 13.27 wt%), SiO<sub>2</sub> (52.62 – 54.88 wt%), Al<sub>2</sub>O<sub>3</sub> (11.63 – 14.17 wt%), P<sub>2</sub>O<sub>5</sub> (0.049 – 0.097 wt%), TiO<sub>2</sub> (1.20 – 1.38 wt%), MnO (0.07 – 0.12 wt%), and K<sub>2</sub>O (0.05 – 0.17 wt%). The enrichment in LOI content in proximal zones is probably associated with the dominance of chlorite, plus the local presence of supergene goethite or late quartz–carbonate veins. Enrichment in MgO and depletion in CaO are likely related to the replacement of primary plagioclase by hypogene chlorite–epidote in proximal zones.

## Supergene alteration of BIF

Intensely supergene-altered BIF is located along the deformed margins of the BIF1, BIF2, and BIF3 macrobands (Fig. 3). Within these intervals, BIF is intensively brecciated and comprises dark-brown fragments of supergene goethite-altered BIF. High-grade ore in the BIF1 macroband (25–30 m) is associated with the dissolution or replacement of primary silica-rich bands by ochreous and vitreous goethite. Iron oxide-rich bands are martite and goethite rich, whereas hypogene magnetite is mainly replaced by martite (indicated by corresponding low magnetic susceptibility values for this interval). Hypogene specularite and microplaty hematite grains are unaffected by supergene alteration. Dissolution of quartz creates a secondary porosity in the rock. Compared with hypogene-altered BIF, the supergene-modified zones are enriched in Fe<sub>total</sub> (56.90 – 64.22 wt%) and depleted in SiO<sub>2</sub> (1.94 – 12.06 wt%), but display comparable values for Al<sub>2</sub>O<sub>3</sub> (0.58 – 1.65 wt%), P<sub>2</sub>O<sub>5</sub> (0.096 – 0.124 wt%), and LOI content (3.72 – 5.64 wt%).

## Supergene alteration of mafic igneous rocks

Mafic igneous rocks located within 25 m of the top of the drillhole (i.e. Mafic1) are intensely supergene altered (Fig. 3).

Intense supergene alteration is more localized beneath the BIF1 macroband where it is spatially associated with the deformed margins of narrow BIF macrobands and discrete brittle–ductile shear zones, or fault zones (e.g. from 184 to 192 m).

Supergene-altered mafic igneous rocks are red brown, fine grained, locally schistose, and comprise mainly goethite (ochreous and vitreous), cryptocrystalline hematite, and kaolinite. In these alteration zones, primary igneous amphibole, pyroxene, olivine, and plagioclase, and metamorphic epidote and chlorite, are replaced by supergene minerals. Relative to least-altered rocks (e.g. Mafic4), the supergene-altered Mafic1 unit is enriched in Al<sub>2</sub>O<sub>3</sub> (22.63 – 32.22 wt%) and LOI content (8.58 – 14.72 wt%), but depleted in SiO<sub>2</sub> (32.95 – 57.10 wt%), P<sub>2</sub>O<sub>5</sub> (0.005 – 0.062 wt%), TiO<sub>2</sub> (0.41 – 0.62 wt%), MgO (0.03 – 0.45 wt%), MnO (0.005 – 0.02 wt%), and CaO (0.02 – 6.15 wt%), and displays comparable values for Fe<sub>total</sub> (5.97 – 18.37 wt%) and K<sub>2</sub>O (0.04 – 0.73 wt%).

## Results of hyperspectral data acquisition and processing

### Method

A detailed description of the general principles of the HyLogger-3 is provided by Hancock et al. (2013) and Duuring and Laukamp (2016a). The HyLogger-3 hyperspectral scanning system developed by CSIRO in Australia uses reflectance spectra of scanned diamond drillcore to identify mineral abundances and mineral chemistry (Hunt, 1977; Clark and Roush, 1984). The HyLogger-3 operated by GSWA in Perth detects radiation reflected from the drillcore within the visible to near infrared (VNIR, 380–1000 nm), short wave infrared (SWIR, 1000–2500 nm) and thermal infrared (TIR, 6000–14000 nm) parts of the electromagnetic spectrum. The HyLogger-3 uses an automated x–y table that moves the core tray at intervals of 1 cm data resolution (Haest et al., 2012a). The reflectance spectra are cross-calibrated using a Spectralon panel. During the nondestructive scanning process, the HyLogger-3 also captures high-resolution digital core images, which are referenced to a standard set of Munsell colours. The hyperspectral data are then processed to determine the abundance of minerals, as well as their composition and/or crystallinity, based on the wavelength, depth and width of diagnostic absorption features. Algorithms applied in this project were developed by CSIRO (Laukamp, 2011; Haest et al., 2012a; Sonntag et al., 2012) and were used in this study to determine mineral abundance and composition of iron oxides, including hematite, vitreous goethite and ochreous goethite, and other minerals such as chlorites, carbonates, amphiboles, white micas, and kaolin group minerals (Appendix).

The collected VNIR, SWIR, and TIR spectral signatures were processed using the commercial software ‘The Spectral Geologist’ (TSG). Mineral abundance and

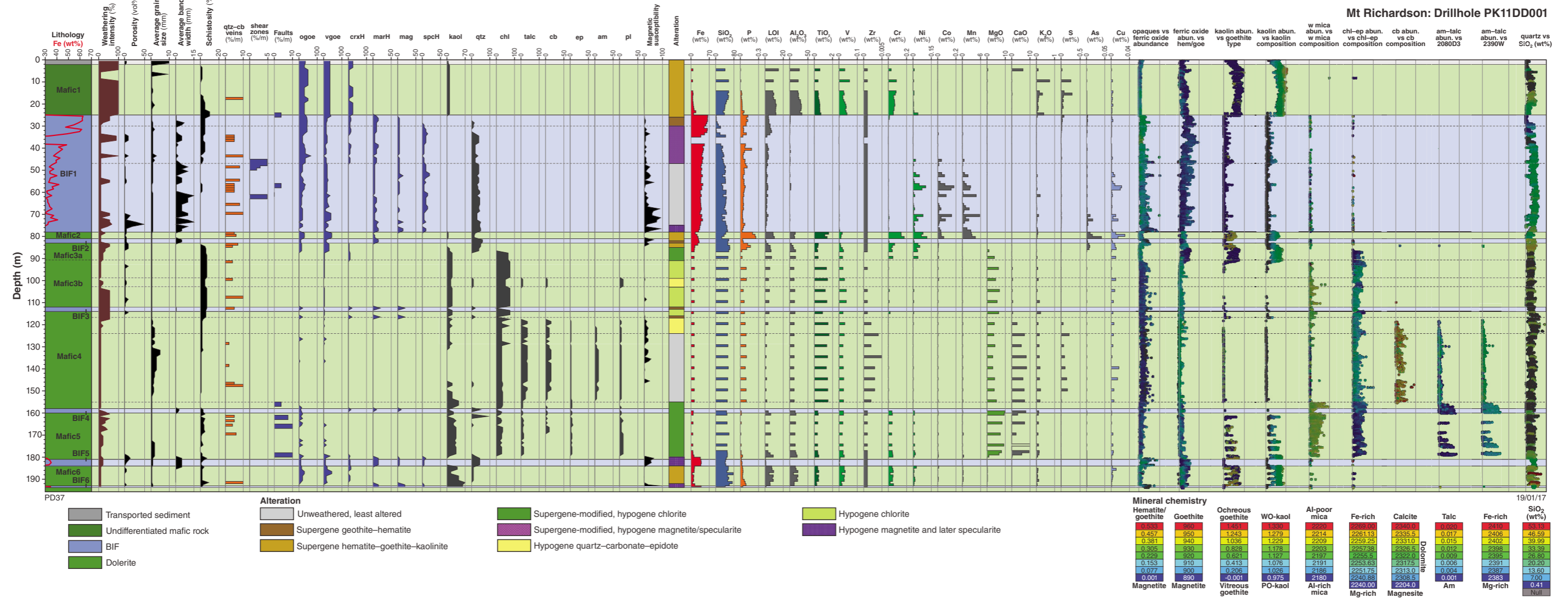
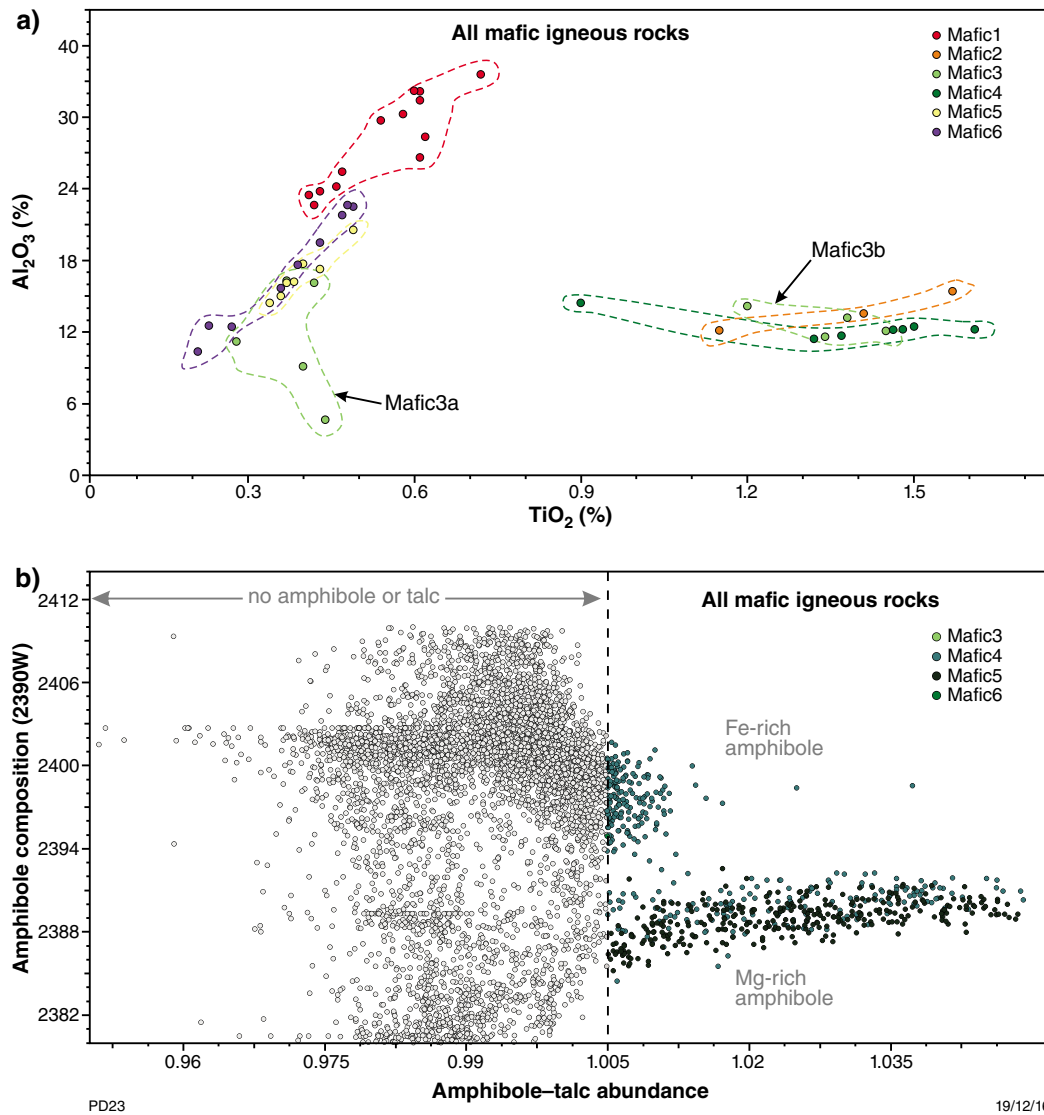


Figure 3. Hyperspectral log for PK11DD001. Abbreviations: abund – abundance; am – amphibole; cb – carbonate; chl – chlorite; crxH – crystalline hematite; ep – epidote; ferric oxide – ferric oxide minerals; goe – goethite; kaol – kaolinite; LOI – loss on ignition; mag – magnetite; marH – martite; ogoe – ochreous goethite; opaques – opaque minerals; pl – plagioclase; PO-kaol – poorly ordered kaolinite; qtz – quartz; spcH – specular hematite; vgoe – vitreous goethite; vol. – volume; w mica – white mica; WO-kaol – well-ordered kaolinite



**Figure 4.** Bulk-rock chemistry and spectral data for mafic igneous rocks: a) immobile element ratios for mafic igneous rocks. Two main compositional groups are demonstrated, both of which display internal fractionation geochemical trends most likely associated with evolution of the magma, combined with the overprinting effects of supergene alteration; b) primary amphibole-talc compositional differences in dolerite units (i.e. Mafic intervals 3–5). Mafic4 contains more Fe-rich amphibole compared with Mafic5.

composition information are extracted using the multiple feature extraction method (Cudahy et al., 2008; Laukamp et al., 2010). Positions and depths of absorption features in this study were calculated by locally removing the hull from the reflectance spectra to reduce the influence of instrument or atmospheric noise (Cudahy et al., 2008).

Reflectance spectral geoscience products that are potentially useful for the study of BIF-hosted iron ore include: 1) opaque minerals (e.g. magnetite and pyrite); 2) ferric oxide minerals (e.g. hematite and goethite); 3) kaolinite composition (e.g. crystalline vs poorly crystalline); 4) white micas (e.g. muscovite and phengite); 5) ferrous iron and magnesium bearing sheet silicates (e.g. actinolite and chlorite); 6) carbonate minerals (e.g. calcite, dolomite, and magnesite; Duuring and Laukamp, 2016a). In all provided examples of reflectance spectral data products, the relative abundance of minerals is indicated by the distribution of the data with vertical depth down the drillhole. The horizontal axes for these plots are without units and show the relative abundance of data. In most plots, the mineral abundance data are coloured on the basis of mineral composition.

## Rock types

Fresh and least-altered mafic rocks can be distinguished from BIF using the high amphibole and plagioclase abundance signatures (e.g. from 124 to 155 m). However, these spectral products are less accurate in areas of drillcore where there is strong replacement of primary amphibole and plagioclase by hypogene and supergene alteration minerals.

Amphibole was detected by the HyLogger-3 only in Mafic4 and Mafic5 intervals (Figs 3, 4b). Amphibole from the Mafic5 interval is exclusively Mg rich, whereas amphibole detected in the Mafic4 interval is a combination of Fe–Mg and Mg rich (Figs 3, 4b). Bulk-rock geochemical data demonstrate that the Mafic5 interval is more MgO-rich than the Mafic4 interval, consistent with the predominance of Mg-rich amphibole in this interval. Immobile element ratios ( $\text{Al}_2\text{O}_3$  vs  $\text{TiO}_2$ ) are also distinctly different between these units (Fig. 4a).

## Hypogene alteration of BIF

Relative to least-altered BIF, the (unweathered) intensely hypogene magnetite-altered BIF at 76–78 m (Fig. 3) displays a higher opaque mineral abundances signature (i.e. enriched in magnetite), but maintains a comparably high quartz abundance signature due to the mutual addition of hypogene magnetite and quartz to BIF during alteration (Fig. 5). Chlorite and white mica are weakly expressed in hypogene-altered BIF.

## Hypogene alteration of mafic igneous rocks

Relative to least-altered dolerite in the Mafic4 interval, unweathered hypogene-altered dolerite proximal to the BIF1 macroband (i.e. Mafic3a) displays an increase in the chlorite abundance index, a corresponding decrease in the detected abundance of amphibole, and chlorite becomes more Mg rich (Figs 3, 6) with proximity to BIF margins (within 13 m of the contact).

More distal zones, such as the Mafic5 interval, have higher whole-rock MgO contents. These rocks also contain primary amphibole and metamorphic or hypogene chlorite that are Mg rich (Fig. 3). The Mg-rich signatures of these rocks are likely inherited from the chemistry of the protolith rather than being the product of hypogene alteration.

## Supergene alteration of BIF

Supergene alteration of BIF, and of hypogene alteration zones, is identified by an increase in the ‘ferric oxide mineral abundance’ and corresponding decreases in the ‘opaque mineral abundance’ and ‘quartz abundance’ signatures (Figs 3, 5). These detected changes are associated with the replacement of primary and hypogene magnetite and quartz by supergene goethite–hematite. Vitreous goethite is dominant over ochreous goethite throughout the BIF1 interval, apart from localized narrow intervals that coincide with weathered dolerite cutting BIF (Fig. 3). Kaolinite is a minor constituent of supergene alteration zones in BIF (Figs 3, 7).

The ‘specularite’ spectral algorithm developed by Chiarelli (2015) reportedly distinguishes specularite from microplaty hematite and martite. However, it is possible that this algorithm more generally identifies hematite and thus overestimates the presence of specularite in this drillhole. Further studies are required to compare spectra from reference samples of pure specularite, microplaty hematite, and martite to test whether they can be distinguished by spectral methods.

## Supergene alteration of mafic igneous rocks

Intense supergene alteration of mafic igneous rocks within the first 25 m of the drillhole (Mafic1) completely replaces primary amphibole, plagioclase, and pyroxene, as well as metamorphic chlorite and epidote, and potential hypogene chlorite. Instead, the interval comprises mainly kaolinite, vitreous goethite, and hematite.

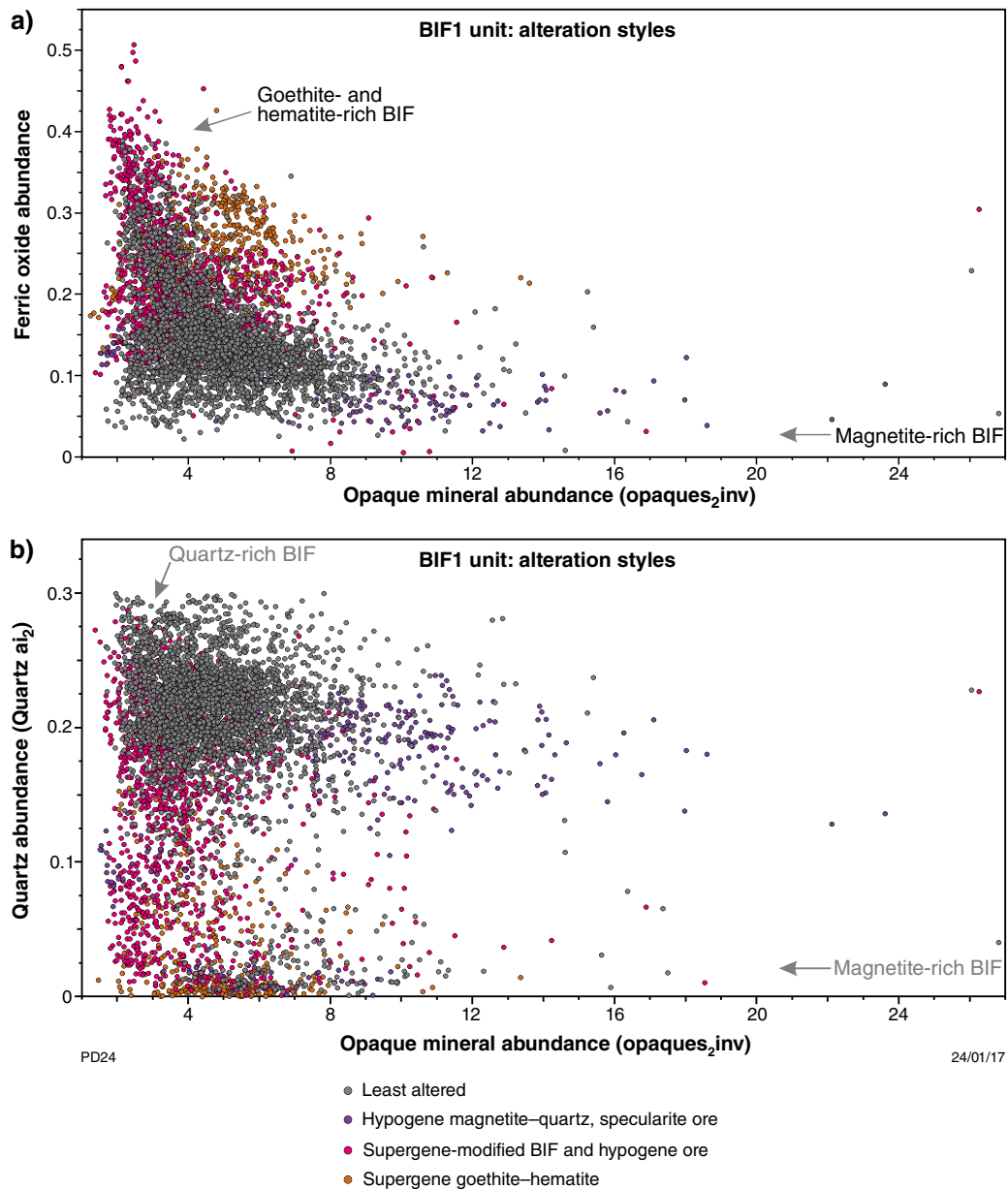


**Figure 5.** Comparison of key indices for least-altered and hypogene- or supergene-altered BIF: a) spectral data demonstrate overlap between altered BIF; however, hypogene-altered BIF displays local enrichment in opaque minerals, corresponding to the addition of hypogene magnetite to BIF; b) quartz abundance does not vary significantly in the hypogene-altered rocks owing to the addition of hypogene quartz with magnetite. In contrast, supergene alteration of least-altered BIF and hypogene-altered BIF results in the oxidation of primary or hypogene magnetite to hematite and goethite, as well as the removal of quartz.

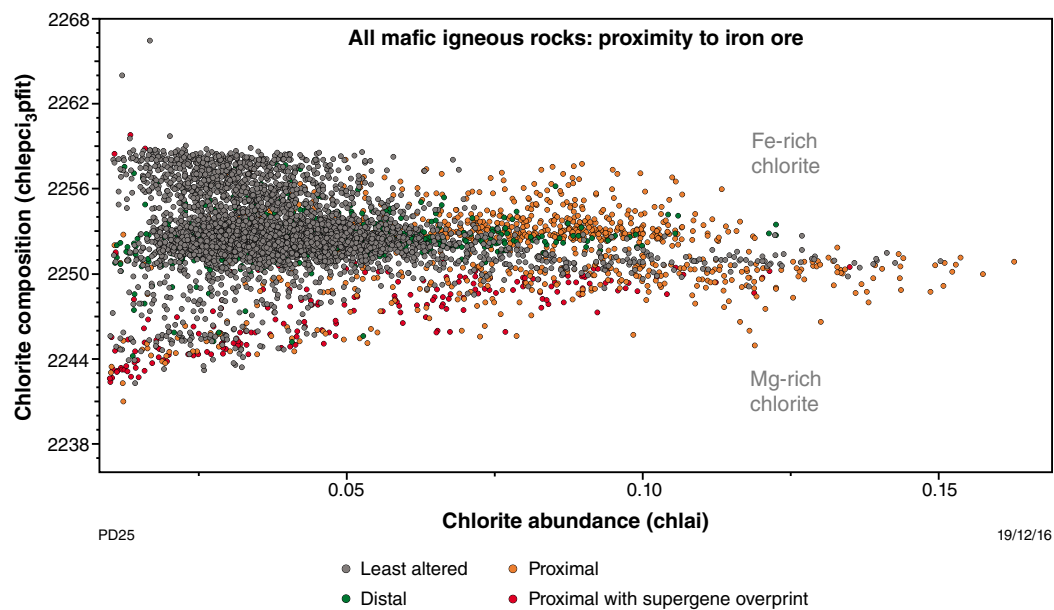


**Figure 6.** Scatter plot showing chlorite abundance vs chlorite composition in all mafic igneous rocks. Chlorite is more abundant and Mg rich in proximal zones compared with more distal areas.

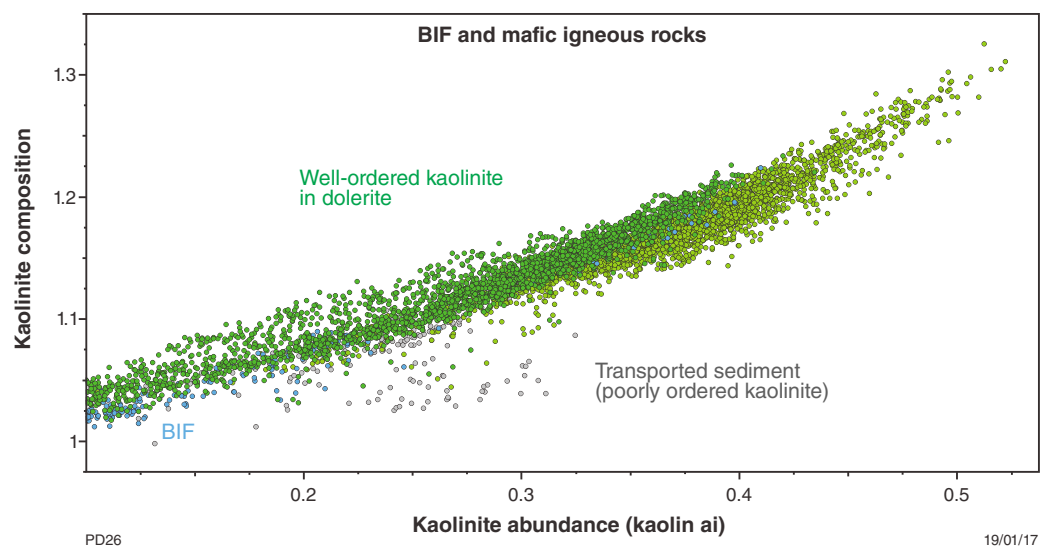


**Figure 7.** Scatter plot showing that transported sediment hosts poorly ordered kaolinite, whereas kaolinite located in situ is well ordered.

Ochreous goethite is restricted to 2–3 m wide shear zones located along contacts with BIF (Fig. 3). Transported sediment in the first 2 m of the drillhole is enriched in poorly ordered kaolinite, whereas underlying in situ occurrences of mafic rocks host well-ordered kaolinite (Fig. 7).

## Conclusions

The PK11DD001 diamond drillhole located in the Parker area of the Mt Richardson iron prospect intersects a 53 m thick BIF macroband and several thinner BIF macrobands. The BIF macrobands are separated by multiple mafic units that vary in thickness and protolith chemistry (demonstrated by differences in their  $\text{Al}_2\text{O}_3/\text{TiO}_2$  ratios). Two main compositional groups are identified: Mafic1, Mafic3a, Mafic5 and Mafic6 intervals are compositionally similar, but are different from Mafic2, Mafic3b and Mafic4. In least-altered mafic igneous rocks, the whole-rock MgO content of the mafic rocks is reflected in the Mg-rich composition of primary amphiboles, as well as metamorphic chlorite.

Fresh examples of least-altered BIF can be distinguished from fresh mafic igneous rocks using spectral scripts that identify amphibole, pyroxene, or plagioclase. However, intense hypogene and supergene alteration that replaces these key indicator minerals hinders the differentiation of these protoliths using their hyperspectral signatures. The spectral signatures of supergene alteration minerals need to be studied in more detail to allow the mapping of the different rock types.

Hypogene alteration in BIF is characterized by the addition of hypogene magnetite and quartz to primary bands. These zones display moderate increases in  $\text{Fe}_{\text{total}}$ , but variably elevated concentrations of  $\text{SiO}_2$  due to the addition of hypogene quartz. Hypogene specularite and microplaty hematite locally replace least-altered BIF and earlier hypogene magnetite-rich ore zones. The oxidation of magnetite to martite is also associated with this hypogene alteration event. It is unclear whether the 'specularite' spectral algorithm developed by Chiarelli (2015) distinguishes between specularite, microplaty hematite, and martite. If this algorithm more generally identifies hematite, then this spectral product most likely overestimates the presence of specularite in this drillhole and would not distinguish between hematite formed by hypogene or supergene processes.

Hypogene alteration zones in mafic rocks are characterized by coincident increases in the chlorite abundance and decreases in amphibole abundance spectral signatures within about 15 m of BIF-hosted iron ore zones. Furthermore, chlorite compositions in mafic igneous rocks become more Mg rich with proximity to these ore zones. However, the effect of intense supergene modification prevents the detection of hypogene alteration mineral vectors due to the replacement of primary, metamorphic, and hypogene minerals by goethite, hematite, and kaolinite.

Later supergene alteration has resulted in a decrease in quartz abundance in least-altered BIF and hypogene magnetite–quartz-rich ore zones, due to the replacement of quartz by goethite. These supergene-modified, hypogene ore zones show an increase in the ferric oxides abundance signature relative to unweathered BIF. The late supergene modification of hypogene ore zones is crucial for the upgrade of iron contents to economic concentrations.

## Acknowledgements

This study was funded by the Geological Survey of Western Australia's Exploration Incentive Scheme (a Royalties for Regions initiative). We thank Cliffs Natural Resources for providing access to drillhole PK11DD001.

## References

- Bishop, JL, Lane, MD, Dyar, MD and Brown, AJ 2008, Reflectance and emission spectroscopy study of four groups of phyllosilicates: smectites, kaolinite-serpentines, chlorites and micas: *Clay Minerals*, v. 43, p. 35–54.
- Clark, RN and Roush, TL 1984, Reflectance spectroscopy: Quantitative analysis techniques for remote sensing applications: *Journal of Geophysical Research: Solid Earth*, v. 89, no. B7, p. 6329–6340.
- Cudahy, TJ, Jones, M, Thomas, M, Laukamp, C, Caccetta, M, Hewson, RD, Rodger, AR and Verrall, M 2008, Next generation mineral mapping: Queensland airborne HyMap and satellite ASTER surveys 2006–2008: CSIRO, Open File Report P2007/364, 120p.
- Chiarelli, L 2015, Alteration mineral zonation associated with high-grade BIF-hosted iron ore: mineral mapping using hyperspectral drill core data: *Geological Survey of Western Australia, Record 2015/3*, 156p.
- Duke, E 1994, Near infrared spectra of muscovite, Tschermak substitution, and metamorphic reaction progress: Implications for remote sensing: *Geology*, v. 22, p. 621–624.
- Duuring, P and Hagemann, SG 2013, Controls for iron mineralisation hosted by banded iron-formation in the Mt Richardson district, Yilgarn Craton, Western Australia: The University of Western Australia, Geological Survey of Western Australia (unpublished report), 28p.
- Duuring, P and Laukamp, C 2016a, Mapping iron ore alteration patterns in banded iron-formation using hyperspectral data: Beebyn deposit, Yilgarn Craton, Western Australia: Geological Survey of Western Australia, Record 2016/16, 18p.
- Duuring, P and Laukamp, C 2016b, Mapping iron ore alteration patterns in banded iron-formation using hyperspectral data: Windarling iron camp, Yilgarn Craton, Western Australia: Geological Survey of Western Australia, Record 2016/17, 14p.
- Geological Survey of Western Australia 2016, 1:500 000 State interpreted geology of Western Australia, 2016: Geological Survey of Western Australia, digital data layer, <www.dmp.wa.gov.au/geoview>.
- Haest, M, Cudahy, T, Laukamp, C and Gregory, S 2012a, Quantitative mineralogy from infrared spectroscopic data. (I) Validation of mineral abundance and composition scripts at the Rocklea channel iron deposit in Western Australia: *Economic Geology*, v. 107, no. 2, p. 209–228.
- Haest, M, Cudahy, T, Laukamp, C and Gregory, S 2012b, Quantitative mineralogy from visible to shortwave infrared spectroscopic data. (II) Three-dimensional mineralogical characterisation of the Rocklea channel iron deposit, Western Australia: *Economic Geology*, v. 107, no. 2, p. 229–249.

- Hancock, EA, Green, AA, Huntington, JF, Schodlok, MC and Whitbourn, LB 2013, HyLogger-3: Implications of adding thermal-infrared sensing: Geological Survey of Western Australia, Record 2013/3, 24p.
- Hunt, G 1977, Spectral signatures of particular minerals in the visible and near infrared: *Geophysics*, v. 42, no. 3, p. 501–513, doi:10.1190/1.1440721.
- Laukamp, C 2011, Short wave infrared functional groups of rock-forming minerals: CSIRO, Report EP115222, 13p.
- Laukamp, C, Caccetta, M, Chia, J, Cudahy, T, Gessner, K, Haest, M, Liu, YC, Ong, C and Rodger, A 2010, The uses, abuses and opportunities for hyperspectral technologies and derived geoscience information: *AIG Bulletin; Geo-Computing 2010 Conference*, Brisbane, September 2010, no. 51, p. 73–76.
- Laukamp, C, Termin, KA, Pejčic, B, Haest, M and Cudahy, T 2012, Vibrational spectroscopy of calcic amphiboles – applications for exploration and mining: *European Journal of Mineralogy*, v. 24, p. 863–878.
- Sonntag, I, Laukamp, C and Hagemann, SG 2012, Low potassium hydrothermal alteration in low sulfidation epithermal systems as detected by IRS and XRD: An example from the Co-O mine, Eastern Mindanao, Philippines: *Ore Geology Reviews*, v. 45, p. 47–60.

Appendix  
Description of spectral scripts for geoscience products

Product name	Minerals detected	Base algorithm	Filters/Masks	Lower stretch limit	Upper stretch limit (based on UGD1683)	Related publication	Comments on general accuracy
Opaques abundance	Sulfides, carbon black (e.g. ash, magnetite, or Mn oxides)	(R456)/(R1650) OPAQUES_450D1650	albedo @ 1650 nm <30%	0.25: low content	Not specified yet – depending on results from other drillcores		Moderate: errors introduced by a lack of Fe <sup>3+</sup> absorption in the visible, e.g. iron oxide poor clays that, in theory, would be masked by the <30% albedo but may be in partial 'shadow'
Ferric oxide abundance (Ferric_oxide_abundance.txt)	Hematite, goethite, jarosite	Continuum removed depth of the 900 nm absorption calculated using a fitted 2nd order polynomial between 776 and 1050 nm. 900D	R450 > R1650	0.04: low content	Not specified – depending on whole dataset	Further developed on the basis of Haest et al. (2012a,b), which used a 4th order polynomial or 4 band ratio approach	Low at Stavely: compromised by other tranistion metal-bearing minerals (e.g. pyroxene). High in regolith and iron ore deposits (Rocklea case study: RMSE = 9.7%)
hem/goe (Hematite-goethite.txt)	Hematite/goethite ratio	Continuum removed wavelength of the 900 nm absorption minimum calculated using a fitted 12th order polynomial between 776 and 1150nm. 900W	R450 > R1650 + 900D >0.025	~900 nm: more hematitic	~940 nm: more goethitic	Haest et al. (2012a,b)	Moderate: wavelength accuracy of the iron-oxide crystal field absorption is adversely affected by mixing with green and dry vegetation as well as ferrous-bearing carbonate and silicate minerals
Kaolin abundance (Kaolin_abundance_2011v2.txt)	Kaolin group minerals: kaolinite halloysite, dickite and nacrite	2200D (Normalized depth of a fitted 4th order polynomial between 2120 and 2245 nm)	2160D [(R2138+R2190)/(R2156+R2179)] >1.005	0.04: low content	Not specified – depending on whole dataset	Sonntag et al. (2012)	High in regolith, low in low-metamorphic grade rocks: compromised by pyrophyllite and prehnite
Kaolin composition (Kaolin_comp_2011v2.txt)	Composition and crystallinity of kaolin group minerals ranging from well-ordered kaolinite to halloysite to dickite (and nacrite)	[(R2138+R2173/R2156)]/[(R2156+R2190)/R2173]	2200D>0.005	Not specified yet – depending on results from other drillcores	Not specified – depending on whole dataset	Sonntag et al. (2012)	Moderate, but compromised by pyrophyllite and prehnite
White mica abundance (wmAlsmat.txt)	Abundance of white micas (e.g. illite, muscovite, paragonite, brammalite, phengite, lepidolite, margarite) and smectites (montmorillonite, beidellite)	Relative absorption depth of the 2200 nm absorption for which the continuum is removed between 2120 and 2245, determined using a 3 band polynomial fit around the band with the lowest reflectance. 2200D3pfit	(R2326+R2376)/(R2343 + R2359) 2350DE >0.00035) + ((R2138+R2190)/(R2156 + R2179) 2160D2190 <1.063	0.04: low content	Not specified – depending on whole dataset	Further developed on the basis of Sonntag et al. (2012), which used a 4th order polynomial or 4 band ratio approach	Moderate: inherent errors related to the process of masking rather than unmixing. That is, the threshold levels on mask parameters could exclude or include other materials especially for 'lower' levels. In sedimentary rocks at Stavely, problems with overlapping kaolinite
White mica composition (wmAlsmci.txt)	Tschermak substitution of white micas, ranging from paragonite, brammalite, to illite, muscovite to phengite, and smectites, ranging from beidellite to montmorillonite	Minimum wavelength of the 2200 nm absorption for which the continuum is removed between 2120 and 2245, determined using a 3 band polynomial fit around the band with the lowest reflectance. 2200W3pfit	(R2326+R2376)/(R2343 + R2359) 2350DE >0.00035) + ((R2138+R2190)/(R2156 + R2179) 2160D2190 <1.063	2185 nm: Al-rich mica (muscovite, illite, paragonite, brammalite, lepidolite)	2220 nm: Al-poor mica (~phengite)	Further developed on the basis of Sonntag et al. (2012), which used a 4th order polynomial or 4 band ratio approach	High: internationally established parameter for tracking Tschermak exchange in white micas and Al-smectites (e.g. Duke, 1994)
Chlorite–epidote abundance (chlepal3pfit.txt)	Chlorite, epidote, biotite	Relative absorption depth of the 2250 nm absorption for which the continuum is removed between 2230 and 2270, determined using a 3 band polynomial fit around the band with the lowest reflectance. 2250D3pfit	2250D3pfit >0.01, 2230 nm < 2250W < 2270 nm	0.04: low content	Not specified – depending on whole dataset	Further developed on the basis of Sonntag et al. (2012), which used a 4th order polynomial or 4 band ratio approach	Moderate: can be influenced by abundant jarosite, tourmaline, phlogopite. Probably some correlation with ferrous iron abundance
Chlorite–epidote composition (chlepci3pfit.txt)	Chlorite, epidote, biotite	Relative absorption depth of the 2250 nm absorption for which the continuum is removed between 2230 and 2270, determined using a 3 band polynomial fit around the band with the lowest reflectance. 2250D3pfit	2250D3pfit >0.01, 2230 nm < 2250W < 2270 nm	2248 nm: Mg-rich (Bishop et al., 2008)	2261 nm: Fe-rich (Bishop et al., 2008)	Further developed on the basis of Sonntag et al. (2012), which used a 4th order polynomial or 4 band ratio approach	Moderate: can be influenced by abundant jarosite, tourmaline, phlogopite. Probably some correlation with ferrous iron abundance
Carbonate abundance index TIR (6500P_3pfit.txt)	Calcite, dolomite, magnesite, siderite, ankerite	6500P Relative height of the reflectance peak between 6300 and 6700 nm, determined using a 3 band polynomial fit around the band with the highest reflectance		0.1	Not specified – depending on whole dataset	Inherited, unpublished	High, but lower threshold dependent on dataset
Carbonate composition index TIR1 (14000DW_3pfit.txt)	Calcite, dolomite, magnesite, siderite, ankerite	14000DW Minimum wavelength of the reflectance low between 13000 and 14000 nm, determined using a 3 band polynomial fit around the band with the lowest reflectance		13000 nm: Mg/Fe-rich	14000 nm: Ca-rich	Inherited, unpublished	High, but lower threshold dependent on dataset
Carbonate abundance (Carbonate_abundance_SWIR.txt)	Carbonates vs MgOH-bearing silicates, based on left-asymmetry of CO <sub>3</sub> feature @ 2340	Relative absorption depth of the 2340 nm absorption for which the continuum is removed between 2270 and 2370, determined using a 3 band polynomial fit around the band with the lowest reflectance. 2340D	2340D >0.04, 2295 nm < 2340W < 2360 nm, 2250D < 0.025, 2380D < 0.1117*2340D + 0.0002. Asymmetry of the 2340 absorption using a fitted 4th order polynomial between 2120 and 2370: 2340_left_asym > 1.13	0.05: low content	Not specified – depending on whole dataset	Further developed on the basis of Sonntag et al. (2012), which used a 4th order polynomial or 4 band ratio approach	Low: heavily impacted by grain size effects. False positives in case of mineral mixtures of, for example, white mica and chlorite
Carbonate composition SWIR (Carbonate_composition_SWIR.txt)	Separating calcite, dolomite, and siderite	Minimum wavelength of the 2340 nm absorption for which the continuum is removed between 2270 and 2370, determined using a 3 band polynomial fit around the band with the lowest reflectance. 2340W	2340D >0.04, 2295 nm < 2340W < 2360 nm, 2250D < 0.025, 2380D < 0.1117*2340D+0.0002, Asymmetry of the 2340 absorption using a fitted 4th order polynomial between 2120 and 2370: 2340_left_asym > 1.13	2303 nm: magnesite; 2326 nm: dolomite; recommendation for Stavely dataset: 2320 nm	2343 nm: calcite; recommendation for Stavely dataset: 2320 nm	Further developed on the basis of Sonntag et al. (2012), which used a 4th order polynomial or 4 band ratio approach	Moderate: works well for those carbonates, which are not masked out by the carbonate abundance index SWIR, The latter should be replaced by carbonate abundance index TIR
Amphibole–talc abundance (Amph_Talc_abundance.txt)	Abundance of amphibole and talc	2380D [(R2365+R2415)/(R2381+R2390)]	Composite mask* + MgOH abundance > 1.01 (+ 2160D2190 < 1.005)	1.005: low content	Not specified – depending on whole dataset	Laukamp et al. (2012)	Moderate: can be compromised by abundant phlogopite; noise
2080D3 (2080D3pfit.txt)	Depth of the 2080 feature, evident in talc. Useful for separating talc from amphiboles, the latter in general not showing this absorption feature	Depth of the 2080 nm absorption feature, for which the continuum is removed between 2060 and 2100, determined using a second order polynomial fitted through the 3 bands with the lowest reflectance. 2080D				Laukamp et al. (2012)	
2390W (2390W3pfit.txt)	Estimate of the Mg/Fe ratio (Mg#) in, for example, amphiboles and talc	Wavelength of absorption minimum calculated using a fitted fourth order polynomial between 2365 and 2430 nm, focused between 2380 and 2410 nm. 2390W		2382 nm: Mg-rich (Laukamp et al., 2012)	2406 nm: Fe-rich (Laukamp et al., 2012)	Laukamp et al. (2012)	
Quartz abundance	Quartz	8635D Relative depth of the 8626 nm Reststrahlen feature for which the continuum is removed between 8565 and 8705 nm, determined using a 3 band polynomial fit around the band with the lowest reflectance	no mask	0.1	Not specified – depending on whole dataset	Inherited, unpublished	High, but lower threshold dependent on dataset. Fractured drillcore can lead to extreme overestimation

References:

Bishop, J.L, Lane, MD, Dyar, MD and Brown, AJ 2008, Reflectance and emission spectroscopy study of four groups of phyllosilicates: smectites, kaolinite-serpentines, chlorites and micas: Clay Minerals, v. 43, p. 35–54

Duke, E 1994, Near infrared spectra of muscovite, Tschermak substitution, and metamorphic reaction progress: Implications for remote sensing: Geology, v. 22, p. 621–624.

Haest, M, Cudahy, T, Laukamp, C and Gregory, S 2012a, Quantitative mineralogy from visible to shortwave infrared spectroscopic data. (I) Validation of mineral abundance and composition products of the Rocklea Dome channel iron deposit in Western Australia: Economic Geology, v. 107, p. 209–228.

Haest, M, Cudahy, T, Laukamp, C and Gregory, S 2012b, Quantitative mineralogy from visible to shortwave infrared spectroscopic data. (II) Three-dimensional mineralogical characterisation of the Rocklea Dome channel iron deposit, Western Australia: Economic Geology, v. 107, p. 229–249.

Laukamp, C, Termin, KA, Pejčic, B, Haest, M and Cudahy, T 2012, Vibrational spectroscopy of calcic amphiboles – applications for exploration and mining: European Journal of Mineralogy, v. 24, p. 863–878.

Sonntag, I, Laukamp, C and Hagemann, S 2012, Low potassium hydrothermal alteration in low sulfidation epithermal systems as detected by IRS and XRD: an example from the Co-O Mine, Eastern Mindanao, Philippines: Ore Geology Reviews, v. 45, p. 47–60.

This Record is published in digital format (PDF) and is available as a free download from the DMP website at  
<[www.dmp.wa.gov.au/GSWApublications](http://www.dmp.wa.gov.au/GSWApublications)>.

Further details of geological products produced by the Geological Survey of Western Australia can be obtained by contacting:

Information Centre  
Department of Mines and Petroleum  
100 Plain Street  
EAST PERTH WESTERN AUSTRALIA 6004  
Phone: +61 8 9222 3459 Fax: +61 8 9222 3444  
[www.dmp.wa.gov.au/GSWApublications](http://www.dmp.wa.gov.au/GSWApublications)

MAPPING IRON ORE ALTERATION PATTERNS IN BANDED  
IRON-FORMATION USING HYPERSPECTRAL DATA:  
DRILLHOLE PK11DD001, MT RICHARDSON,  
YILGARN CRATON, WESTERN AUSTRALIA

